Dynamics of Bubbles Moving in Liquids with Pressure Gradient

HSU-CHIEH YEH AND WEN-JEI YANG
Department of Mechanical Engineering, The University of Michigan, Ann Arbor, Michigan
(Received 11 December 1967; in final form 5 February 1968)

The time history of the velocity, size, and deformation of a bubble moving in the flow field around a point source or sink is studied analytically. Consideration is given to the case where the changes in the bubble velocity, size, and deformation are caused by the dynamic forces of the fluid, rather than the initial perturbation of the bubble shape. The effect of viscosity and gravitation is neglected. The flow is considered irrotational and the velocity potential is assumed to exist. The gas, vapor, or their mixture inside the bubble undergoes a polytropic process. The governing equations for the translatory motion, size, and deformation of the bubble are derived by perturbation theory. The analysis is general and may be applied to an initially spherical as well as nonspherical bubble. It is disclosed that the time history of the bubble's translating velocity in a sink flow is monotonically increasing, while in a source flow it varies following two typical patterns depending upon the initial velocity. In a sink flow, an initially spherical bubble can maintain a nearly spherical shape over a rather long distance as it grows, while in a source flow, the bubble shape varies with time in various ways, depending on the initial velocity. The analysis may also predict, by means of numerical reduction, the moment corresponding to the threshold of instability from which the bubble will attain an irregular shape. The mechanisms leading to the photographically observed behavior of a cavitation bubble moving in a rectangular venturi tube diffuser by Ivany *et al.* (1966) are revealed, in that the flow in a section of such a diffuser (or nozzle) closely resembles source or sink flow.

INTRODUCTION

The problems on the translatory motion and deformation of a bubble have been studied by a number of investigators. However, due to the difficulty and complexity of the problem, those investigations are limited to some special cases: Plesset and Mitchell[1] and Naude and Ellis[2] considered the dynamics of a stationary bubble in quiescent liquids with uniform system pressure. Since the force acting upon the bubble from the surrounding liquid is symmetrical, the instability problem may arise only when the bubble starts to grow or collapse from an initially nonspherical form. Furthermore, since there is no bulk flow of the liquid and the bubble is not in translating motion, the perturbed dynamics equations are not coupled and thus may be solved independently. Hartunian and Sears[3] studied the instability of a translating bubble in a liquid with uniform pressure. They obtained a set of simultaneous coupled equations whose solution may predict the onset of the instability in the bubble's translatory motion. Since the bubble being considered remains constant in size during the course of translating motion, the equations determining instability are independent of time. Walters and Davidson[4] investigated the deformation of bubble shape caused by the translating motion and the pressure gradient in the surrounding liquid. However, since the problem dealt with the case where during the transient, the volume of the bubble and the pressure gradient due to gravitation in the liquid are both constant, the acceleration of the bubble in the liquid is constant and equal to $2g$.

Recently, Ivany *et al.*[5] have photographically studied the dynamics of cavitation bubbles in a liquid flowing through a venturi. They observed "rebound" phenomena in the translating motion, size and deformation of the bubble during the course of its collapse. These phenomena are quite complicated due to the interaction among the liquid flow, the bubble's translating motion, the collapse or growth of the bubble, and the nonuniformity in the pressure gradient.

This paper is the extension of Ref. 3 to the case of motion in a source or sink flow. While Ref. 3 considers the problem of shape instability due to self-induced, asymmetrical disturbances, the present work deals with the dynamic behavior of a moving gas bubble induced by the flow field with a nonuniform pressure gradient. The analysis is general and may include self-induced disturbances into consideration simply by imposing nonzero $a_n(0)$ as the initial conditions of Eqs. (29), which appear later in the text. Throughout the paper "gas" refers to the gas, vapor, or their mixture in the bubble, unless otherwise stated. Consideration is given to the cases where the surrounding liquid is a source flow, a sink flow, or their combination. The problem is simplified through the assumptions of constant liquid density, negligible effects of heat and mass transfer, and polytropic processess for the fluid inside the bubble in translatory motion in an ideal liquid flow. The effect of gravitation is also neglected. Analytical results are obtained for the time history of the bubble's size, shape, and translational velocity. The characteristic behavior of a translating gas bubble

[1] M. S. Plesset and T. P. Mitchell, Quart. Appl. Math. **13**, 419 (1956).
[2] C. F. Naude and A. T. Ellis, Trans. ASME J. Basic Engr. **83**, 648 (1961).
[3] R. A. Hartunian and W. R. Sears, J. Fluid Mech. **3**, 27 (1957).
[4] J. K. Walters and J. F. Davison, Pt. 1, J. Fluid Mech. **12**, 408 (1962); Pt. 2, J. Fluid Mech. **17**, 321 (1963).
[5] R. D. Ivany, F. G. Hammitt, and T. M. Mitchell, Trans. ASME Ser. D: J. Basic Eng. **88**, 649 (1966).

disclosed in the study agrees with that observed in Ref. 5.

ANALYSIS

For an incompressible fluid, the equation of continuity can be written as

$$\nabla \cdot \mathbf{V} = 0, \tag{1}$$

where $\mathbf{V}$ is the velocity vector. If the flow is irrotational then the velocity potential Φ exists, that is,

$$\mathbf{V} = -\nabla\Phi,$$

and Eq. (1) becomes

$$\nabla^2\Phi = 0. \tag{2}$$

Consider a bubble in translatory motion with the velocity V_1 in the flow field of a point source of strength μ ($\mu>0$ indicates a source, $\mu<0$ indicates a sink). At time t, the bubble is located at distance r_1 from the source, as illustrated in Fig. 1. Under these circumstances, the bubble surface is subject to nonuniform pressure from the surrounding liquid. As a result, an initially spherical bubble cannot retain a spherical shape as it travels with the flow. It is postulated that bubble shape may be expressed in the spherical coordinates (r, θ, ϕ) with the origin fixed at the center of the bubble and moving with the bubble as

$$r_s(t, \theta) = R(t) + \sum_{n=1}^{\infty} a_n(t) P_n(\cos\theta), \tag{3}$$

in which r_s is the radial distance from the center to the surface of the bubble, $R(t)$ is the radius of unperturbed bubble, a_n are the time varying coefficients to be determined, $P_n(\cos\theta)$ are the Lengendre polynomials, and θ is the angle measured from the reference line, defined as connecting the bubble center and the point source (Fig. 1). Then the solution of Eq. (2), in moving coordinate systems at an arbitrary location $P(r, \theta, \phi)$ in the flow field, may be obtained as

$$\Phi = \mu \sum_{n=0}^{\infty} \frac{r_<^n}{r_>^{n+1}} P_n(\cos\theta) - V_1 r\cos\theta + \sum_{n=0}^{\infty} \frac{b_n}{r^{n+1}} P_n + \sum_{n=1}^{\infty} \frac{c_n}{r^{n+1}} P_n, \tag{4}$$

where $r_<$ equals r if $r<r_1$, or $r_<$ equals r_1 if $r>r_1$; $r_>$ equals r if $r>r_1$ or $r_>$ equals r_1 if $r<r_1$. The constant coefficients b_n and c_n are to be determined. Equation (4) indicates that the velocity potential consists of four components. The first term on the right side of Eq. (4) expresses the velocity potential at P in the absence of the bubble. The second term, $-V_1 r\cos\theta$, signifies the component induced by the motion of the coordinates. The third term,

$$\sum_{n=0}^{\infty} \frac{b_n}{r^{n+1}} P_n,$$

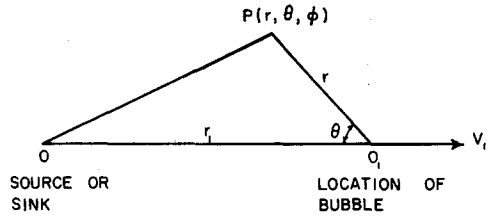

FIG. 1. Coordinate systems for analyzing the dynamics of a bubble moving in a source or sink flow.

is the contribution to the velocity potential due to the presence of a spherical bubble with radius $R(t)$. Therefore, the coefficients b_n are determined by substituting Eq. (4), without the last term, into the condition

$$\dot{R}(t) = -(\partial\Phi/\partial r)_{r=R}, \tag{5}$$

where the dot denotes the time derivative. It is followed by comparing terms of the resulting equation. Now, Eq. (4) may be rewritten as

$$\Phi = \mu \sum_{n=0}^{\infty} \frac{r_<^n}{r_>^{n+1}} P_n - V_1 r\cos\theta + \frac{R^2\dot{R}}{r} + \frac{R^3}{2r^2}\left(\frac{\mu}{r_1^2} - V_1\right) \times\cos\theta + \sum_{n=2}^{\infty} \frac{n\mu R^{2n+1}}{(n+1)(rr_1)^{n+1}} P_n + \sum_{n=1}^{\infty} \frac{c_n}{r^{n+1}} P_n. \tag{6}$$

The last term

$$\sum_{n=1}^{\infty} \frac{c_n}{r^{n+1}} P_n$$

of Eq. (4) expresses the component induced by the deviation of the bubble shape from a spherical form. The determination of the coefficients c_n is explained below.

If the surface of the perturbed bubble (3) is represented by

$$F(r_s, \theta, t) = r_s - R - \sum_{n=1}^{\infty} a_n P_n = 0; \tag{7}$$

then it requires that the condition

$$DF/Dt = \partial F/\partial t + (V_\theta)_{r=r_s}(1/r_s)(\partial F/\partial\theta) + (V_r)_{r=r_s}\partial F/\partial r_s = 0 \tag{8}$$

be satisfied at the bubble surface. In Eq. (8), V_r and V_θ are the velocity components defined as $-\partial\Phi/\partial r$ and $-(1/r)\partial\Phi/\partial\theta$, respectively. Now, Eq. (6) is substituted into Eq. (8) followed by comparing terms multiplied by P_n. It must be noted that the second- or higher-order terms involving a_n and R_1/r are neglected. The neglect of higher-order terms of a_n will be justified later from the numerical evaluation of the a_n. The higher-order terms involving R/r_1 may be negligible if the distance between the bubble and the source or sink is large compared with the bubble radius. Now, using the recurrence formulas for $\sin^2\theta P_n'$, $\cos\theta P_n$ and

P_2P_n,[6,7] one obtains

$$\Phi=\sum_{n=0}^{\infty}\frac{\mu r_<^n}{r_<^{n+1}}P_n-V_1r\cos\theta+\frac{R^2\dot{R}}{r}\frac{R^3}{2r^2}\left(\frac{\mu}{r_1^2}-V_1\right)\cos\theta+\sum_{n=2}^{\infty}\frac{n\mu R^{2n+1}}{(n+1)(rr_1)^{n+1}}P_n$$

$$-\sum_{n=3}^{\infty}\frac{5n(n-2)}{(2n-1)(2n+1)}\frac{\mu R^n}{r_1^3r^{n-1}}a_nP_{n-2}-\sum_{n=2}^{\infty}\tfrac{1}{2}\frac{n(n-1)}{2n+1}\left(\frac{R}{r}\right)^n\left(\frac{\mu}{r_1^2}-V_1\right)a_nP_{n-1}$$

$$+\sum_{n=1}^{\infty}\frac{5n}{(2n-1)(2n+3)}\frac{\mu R^{n+2}}{r_1^3r^{n+1}}a_nP_n+\sum_{n=1}^{\infty}\frac{1}{n+1}\frac{R^{n+2}}{r^{n+1}}\left(\dot{a}_n+2\dot{R}\frac{a_n}{R}\right)P_n$$

$$+\tfrac{3}{2}\sum_{n=1}^{\infty}\frac{(n+1)R^{n+2}}{(2n+1)r^{n+2}}\left(\frac{\mu}{r_1^2}-V_1\right)a_nP_{n+1}+15\sum_{n=1}^{\infty}\frac{(n+1)(n+2)\mu R^{n+4}}{(n+3)(2n+1)(2n+3)r_1^3r^{n+3}}a_nP_{n+2}. \quad (9)$$

This result includes the special cases of Refs. 1–3, e.g., Eq. (9) for $\mu=0$ and $V_1=0$ reduces to the case analyzed in Ref. 1.

Next, the equation of motion for an irrotational flow may be written in an accelerating coordinate system, as

$$\nabla(-\partial\Phi/\partial t+V^2/2+p/\rho)=-\mathbf{a}, \quad (10)$$

where $\mathbf{a}$ is the acceleration vector of the coordinate system. Its r-component equation

$$(\partial/\partial r)(-\partial\Phi/\partial t+V^2/2+p/\rho)=-a_r,$$

where $a_r=-(dV_1/dt)\cos\theta$ in the system shown by Fig. 1, is integrated from the bubble surface $r=r_s$ to infinity $r=\infty$. The pressure distribution on the bubble surface results as

$$p(r_s)=p(\infty)+\rho\left[-\partial\Phi/\partial t+(V^2/2)\right]_{r=r_s}^{r=\infty}-\rho(dV/dt)\left[r\cos\theta\right]_{r=r_s}^{r=\infty}, \quad (11)$$

where $V^2/2$, the kinetic energy per unit mass, is

$$\tfrac{1}{2}V^2=\tfrac{1}{2}(-\nabla\Phi)^2. \quad (12)$$

The $\partial\Phi/\partial t$ term may be evaluated with the aid of Eq. (9). It is found that

$$(\partial\Phi/\partial t)_{r=\infty}=-((dV_1/dt)r\cos\theta)_{r=\infty}, \quad (13)$$

which cancels out the upper limit of the last term of Eq. (11). Equations (12) and (9) yield

$$\tfrac{1}{2}V^2=\tfrac{1}{2}V_1^2,$$

as $r\to\infty$, which is to be expected for a moving coordinate system. One can also write

$$((dV_1/dt)r\cos\theta)_{r=r_s}=(dV_1/dt)\left(R+\sum_{n=1}^{\infty}a_nP_n\right)\cos\theta. \quad (14)$$

Since the liquid pressure at infinity is not affected by the presence of the bubble in the flow field, the application of the Bernoulli's equation yields

$$p(\infty)=p_0+\tfrac{1}{2}(\mu/r_0^2)^2, \quad (15)$$

where r_0 is the distance between the bubble and the source or sink at zero time, and p_0 and μ/r_0^2 are the liquid pressure and velocity, respectively, at $r=r_0$. Thus, $p(r_s)$, the liquid-pressure distribution over the bubble surface

[6] P. M. Morse and H. Feshbach, *Methods of Theoretical Physics* (McGraw-Hill Book Company, New York, 1953), Chap. 10, p. 1326.

[7] E. T. Whittaker and G. N. Watson, *Modern Analysis* (Cambridge University Press, New York, 1927), 4th ed., Chap. 15, p. 331.

may be evaluated by substituting Eqs. (9) and (12)–(15) into Eq. (11). It yields

$$\frac{p(r_s)}{\rho}=R\ddot{R}+\tfrac{3}{2}\dot{R}^2+\frac{p_0}{\rho}+\frac{1}{2}\left[\left(\frac{\mu}{r_0^2}\right)^2-\left(\frac{\mu}{r_1^2}\right)^2\right]-\frac{1}{4}\left(\frac{\mu}{r_1^2}-V_1\right)^2+\left[-\tfrac{1}{2}R\frac{dV_1}{dt}+\tfrac{3}{2}\dot{R}\left(\frac{\mu}{r_1^2}-V_1\right)-3\frac{\mu R}{r_1^3}V_1\right]\cos\theta$$
$$+\frac{3}{4}\left(\frac{\mu}{r_1^2}-V_1\right)^2P_2-\tfrac{5}{2}\sum_{m=0}^{\infty}\frac{(m+1)(m+2)}{2m+3}\left(\frac{\mu}{r_1^2}\right)^2\left(\frac{R}{r_1}\right)^{m+2}P_m-\tfrac{3}{2}\sum_{m=1}^{\infty}(m+1)\left(\frac{\mu}{r_1^2}-V_1\right)\frac{\mu}{r_1^2}\left(\frac{R}{r_1}\right)^m P_m$$
$$+\sum_{m=2}^{\infty}(2m+1)\frac{\mu}{r_1^2}\left[-\left(\frac{R}{r_1}\right)^m V_1+\frac{m}{m+1}\left(\frac{R}{r_1}\right)^{m-1}\dot{R}-\frac{5}{2}\frac{m}{(2m-1)(2m+3)}\left(\frac{R}{r_1}\right)^m\frac{\mu}{r_1^2}\right]P_m$$
$$+\tfrac{3}{2}\sum_{m=3}^{\infty}(2m-1)\left(\frac{\mu}{r_1^2}-V_1\right)\frac{\mu}{r_1^2}\left(\frac{R}{r_1}\right)^{m-2}P_m+\cdots. \quad (16)$$

The complete expression of Eq. (16) is not presented here because of its length, but is available in Ref. 8.

In order to determine the time history of bubble's translatory motion, the bubble surface is defined as the control surface. Let $\mathbf{n}$ be the unit normal vector at a point (r_s, θ, ϕ) on the bubble surface as shown in Fig. 2. Then its components in the r_s, θ, and ϕ direction are $F_{r_s}/[F_{r_s}^2+(F_\theta/r_s)^2]^{1/2}$, $(F_\theta/r_s)/[F_{r_s}^2+(F_\theta/r_s)^2]^{1/2}$, and 0, respectively, where the subscripts r_s and θ denote the derivatives with respect to r_s and θ, respectively. If β is defined as the angle between the normal vector $\mathbf{n}$ and the radial vector $\mathbf{r}_s$ on the bubble surface, then the r_s and θ components of $\mathbf{n}$ become

$$F_{r_s}/[F_{r_s}^2+(F_\theta/r_s)^2]^{1/2}=\cos(\mathbf{n},\mathbf{r}_s)=\cos\beta \quad (17)$$

and

$$(F_\theta/r_s)/[F_{r_s}^2+(F_\theta/r_s)^2]^{1/2}=\cos(\mathbf{n},\boldsymbol{\theta})=-\sin\beta, \quad (18)$$

respectively. The combination of Eqs. (7), (17), and (18) produces

$$\cos\beta\cong 1 \quad (19a)$$

and

$$\sin\beta\cong=R^{-1}\sum_{n=1}^{\infty}a_nP_n'\sin\theta. \quad (19b)$$

Now, since there is no mass transfer across the control surface, Newton's second law of motion can be written as

$$f=-m_1dV_1/dt, \quad (20)$$

where m_1 is the mass of the gas inside the bubble and f is the z-direction force induced by the pressure extending on the control surface, which may be expressed as

$$f=-\int_m p(r_s)\cos(\theta-\beta)dA, \quad (21)$$

where A is the area of the bubble surface and $\theta-\beta$ is the angle of the directions of the liquid pressure and the z axis (See Fig. 2.). With the aid of Eq. (19), the quantity $\cos(\theta-\beta)$ in the integrand of Eq. (21) may be approximated as

$$\cos(\theta-\beta)\cong\cos\theta+R^{-1}\sum_{n=1}^{\infty}a_nP_n'\sin^2\theta, \quad (22)$$

where the prime denotes the derivative with respect to $\cos\theta$. dA on the bubble surface may be expressed as

$$dA=2\pi r_s\sin\theta[r_s^2+(dr_s/d\theta)^2]^{1/2}d\theta.$$

Since

$$\frac{dr_s}{d\theta}=-\sum_{n=1}^{\infty}a_nP_n'\sin\theta,$$

it becomes obvious that the $(dr_s/d\theta)^2$ term consists of the terms all involving a_n^2. The $(dr_s/d\theta)^2$ term is, therefore, considered small in comparison with the r_s^2 term and the differential area dA is approximated by

$$dA\cong 2\pi R^2[1+2\sum_{n=1}^{\infty}(a_n/R)P_n]\sin\theta d\theta. \quad (23)$$

By substituting Eqs. (22) and (23) into Eq. (21) and neglecting m_1 in Eq. (20), one obtains

$$2\pi R^2\int_0^\pi p(r_s)\left[\cos\theta-\sum_{n=2}^{\infty}\frac{(n-3)n}{2n-1}\frac{a_{n-1}}{R}P_n+\sum_{n=0}^{\infty}\frac{(n+1)(n+4)}{2n+3}\frac{a_{n+1}}{R}P_n\right]d(\cos\theta)=0. \quad (24)$$

Now, Eq. (16) for $p(r_s)$ is substituted into Eq. (24),

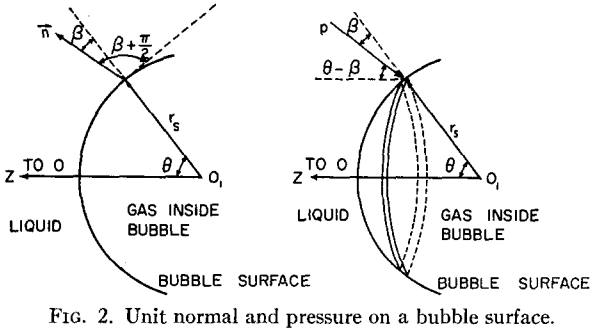

FIG. 2. Unit normal and pressure on a bubble surface.

[8] H. C. Yeh, Ph. D. thesis, Mech. Engr. Dept., The University of Michigan (1967).

followed by performing integration utilizing the orthogonality property of Legendre polynomials:

$$\int_{-1}^{1} P_n(u)\,P_m(u)\,du = 2/(2n+1) \qquad \text{if } n=m$$
$$= 0 \qquad \text{if } n\neq m.$$

Hence, there results the expression for the bubble's translating motion, which predicts r_1 and $V_1(=dr_1/dt)$:

$$\frac{1}{3}\frac{dV_1}{dt}R-\dot{R}B+2\frac{\mu^2}{r_1^4}\left(\frac{R}{r_1}\right)+2\frac{\mu^2}{r_1^4}\left(\frac{R}{r_1}\right)^3-\tfrac{1}{3}R\ddot{a}_1-\left(\dot{R}-\frac{2}{3}\frac{\mu}{r_1^2}\frac{R}{r_1}\right)\dot{a}_1$$

$$+\tfrac{1}{3}\ddot{R}a_1+\frac{2}{3}\left(3\frac{\mu\dot{R}}{r_1^3}a_1-3\frac{\mu R}{r_1^4}V_1a_1+\frac{\mu R}{r_1^3}\dot{a}_1\right)+\left(\frac{8}{3}\frac{\mu\dot{R}}{r_1^3}+\frac{6}{5}\frac{B^2}{R}-2\frac{\mu}{r_1^3}B\right)a_1+\frac{56}{3}\left(\frac{\mu}{r_1^2}\right)^2\frac{R}{r_1}a_1$$

$$+\tfrac{2}{5}B\dot{a}_2-\frac{4}{15}\left(\frac{\mu}{r_1^3}V_1+\frac{1}{2}\frac{dV_1}{dt}+\frac{\mu}{r_1^3}B\right)a_2+\frac{4}{7}\frac{\mu R}{r_1^3}\dot{a}_2-\frac{4}{35}\left[-10\frac{\mu\dot{R}}{r_1^3}+\frac{9}{2}\frac{B^2}{R}+30\frac{\mu B}{r_1^3}+\frac{85}{9}\left(\frac{\mu}{r_1^2}\right)^2\frac{R}{r_1^2}\right]a_3$$

$$-\frac{40}{21}\frac{\mu}{r_1^3}Ba_1-\frac{800}{693}\left(\frac{\mu}{r_1^2}\right)^2\frac{R}{r_1^2}a_5+\frac{B^2}{5R}a_1+\frac{2}{7}\frac{\mu R}{r_1^3}\dot{a}_3-\frac{2}{7}\left[\frac{\mu R}{r_1^4}V_1-\frac{\mu\dot{R}}{r_1^3}+3\left(\frac{\mu}{r_1^2}\right)^2\frac{R}{r_1^2}\right]a_3$$

$$-5\sum_{m=2}^{\infty}\frac{(m-3)m(m+1)(m+2)}{(2m-1)(2m+1)(2m+3)}\left(\frac{\mu}{r_1^2}\right)^2\left(\frac{R}{r_1^2}\right)^{m+2}\frac{a_{m-1}}{R}-3\sum_{m=2}^{\infty}\frac{(m-3)m(m+1)}{(2m-1)(2m+1)}\frac{B}{R}\frac{\mu}{r_1^2}\left(\frac{R}{r_1}\right)^m a_{m-1}+\cdots=0, \quad (25)$$

where $B=(\mu/r_1^2)-V_1$. The complete expression of Eq. (25) is available in Ref. 6.

One is now concerned with the time history of the bubble size and shape. The force balance on the differential element of the bubble surface leads to the expression

$$\sigma(R_1^{-1}+R_2^{-1})=p_{\text{in}}(r_s)-p_{\text{out}}(r_s), \quad (26)$$

where σ is the surface tension, R_1 and R_2 are the principal radii of curvature of the bubble surface, and p_{in} and p_{out} are the pressures exerted on the inside and outside surfaces of the bubble, respectively. Assuming that the gas, vapor, or their mixture inside the bubble is ideal and undergoes a polytropic process during the growth or collapse of the bubble, one obtains

$$p_{\text{in}}(t)=p_{\text{in}}(0)[R(0)/R(t)]^{3\gamma}, \quad (27)$$

where $p_{\text{in}}(0)$ is the initial gas pressure and γ is a constant for a polytropic process. For a perturbed sphere the sum of the curvatures up to the first-order correction may be written as

$$R_1^{-1}+R_2^{-1}=\frac{2}{R}+\sum_{n=1}^{\infty}\frac{(n-1)(n+2)}{R^2}a_nP_n. \quad (28)$$

With the substitution of Eqs. (16), (27), and (28) into (26), followed by equating terms involving P_n to zero, there results a set of second-order differential equations for R and a_n: The coefficients of P_0 yield the equation for R as

$$R\ddot{R}+\tfrac{3}{2}\dot{R}^2+\frac{1}{2}\left[\left(\frac{\mu}{r_0^2}\right)^2-\left(\frac{\mu}{r_1^2}\right)^2\right]-\tfrac{1}{4}B^2+\frac{p_0-p_{\text{in}}}{\rho}+\frac{2\sigma}{\rho R^2}$$

$$-\frac{5}{3}\left(\frac{\mu}{r_1^2}\right)^2\left(\frac{R}{r_1}\right)^2+\frac{1}{3}\left[-\tfrac{3}{2}B\dot{a}_1+\left(\dot{V}_1-3\frac{\dot{R}B}{R}+\frac{9B^2}{2R}-\frac{4B\mu}{15r_1^3}\right)a_1\right]$$

$$-\left[\frac{2\mu R}{3r_1^3}\dot{a}_2+\left(-\frac{4\mu\dot{R}}{3r_1^3}+\frac{B^2}{5R}+\frac{3\mu B}{r_1^3}-\frac{10\mu^2R}{21r_1^6}\right)a_2+\frac{6B\mu}{7r_1^3}a_3+\frac{40\mu^2R}{63r_1^6}a_4\right]=0, \quad (29a)$$

where $B=\mu/r_1^2-V_1$.

The coefficients of P_1 yield the equation for a_1 as

$$\tfrac{1}{2}R\ddot{a}_1-\tfrac{1}{2}R\dot{V}+\tfrac{3}{2}\dot{R}B-3\frac{\mu RV_1}{r_1^3}-3\left(\frac{\mu}{r_1^2}\right)^2\left(\frac{R}{r_1}\right)^3-3\frac{B\mu R}{r_1^3}+\tfrac{3}{2}\dot{R}\dot{a}_1$$
$$-\left(\frac{\ddot{R}}{2}+\frac{3\mu RV_1}{r_1^4}+\frac{\mu\dot{R}}{r_1^3}+\frac{9B^2}{5R}-\frac{3\mu B}{r_1^3}+\frac{20R\mu^2}{7r_1^6}\right)a_1-\tfrac{4}{5}B\dot{a}_2$$
$$+\tfrac{1}{5}\left(3\dot{V}_1-\frac{6\dot{R}B}{R}+\frac{27B^2}{2R}+11.12\frac{B\mu}{r_1^3}+\frac{2u}{r_1^3}V_1\right)a_2-\frac{9\mu R}{7r_1^3}\dot{a}_3$$
$$+\frac{1}{7}\left(-\frac{15\mu\dot{R}}{r_1^3}+\frac{27B^2}{5R}+\frac{36\mu B}{r_1^3}-\frac{56.52\mu^2R}{5r_1^6}+\frac{3\mu RV_1}{r_1^4}+\frac{9\mu^2R}{r_1^6}\right)a_3+\frac{20\mu B}{7r_1^3}a_4+\frac{1.73\mu^2R}{r_1^4}a_5=0\,. \quad (29b)$$

These equations are coupled not only among themselves, but also with Eq. (25). Therefore, it is necessary to solve Eq. (29) together with Eq. (25) simultaneously for r_1, R and a_n's.

RESULTS AND DISCUSSION

All physical quantities involving the length, velocity acceleration, time, pressure, and source strength may be nondimensionalized by dividing by R_0, $(\sigma/\rho R_0)^{1/2}$, $\sigma/\rho R_0^2$, $(\rho R_0^3/\sigma)^{1/2}$, σ/R_0, and $(\sigma R_0^3/\rho)^{1/2}$, respectively, where R_0 is the initial radius of the bubble, or $R(0)$. The dimensionless velocity thus defined is exactly the Weber number. With the introduction of these definitions, all equations in the previous section may be nondimensionalized. Each resulting equation retains an identical expression with the corresponding original equation in dimensional form except that ρ and σ are dropped from the new set. In the following discussion we always refer to the equations in dimensionless form.

Equations (25) and (29) were numerically integrated by the Runge-Kutta method using an IBM 7090 digital computer. Twelve equations for a_1, a_2,$\cdots$, up to a_{12} were involved in the numerical reduction.

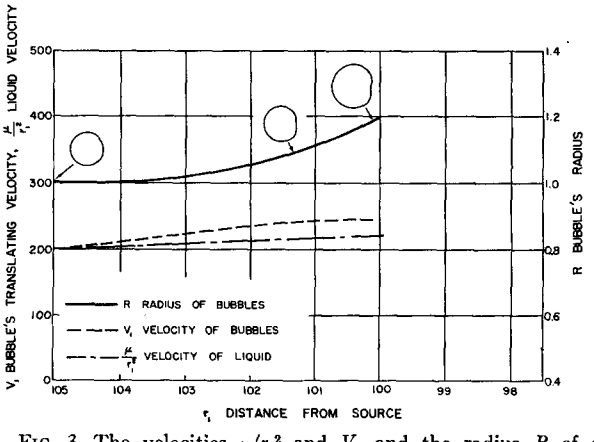

FIG. 3. The velocities μ/r_1^2 and V_1 and the radius R of a spherical bubble moving in a sink flow with the initial conditions $r_0=105$, $R(0)=1$, $V_0=200$, and $p_{in}(0)=4395$. [The bubble shape is predicted by Eqs. (25) and (29).]

All other equations involving a_n with n greater than twelve were considered of higher order of magnitude and thus were ignored. However, it is disclosed from the experimental study that sufficiently accurate results may be obtained by retaining the first 12 equations in the computer program. Altogether, 14 simultaneous equations were programmed in the numerical reduction for r_1, R, and the first 12 a_n. It is assumed for the numerical computation that the bubble at the start of the transient is in a spherical form. This is equivalent to imposing the conditions that all a_n's and $\dot{a}_n$'s are zero and R_0 or $R(0)$ is equal to unity. Under these initial conditions, however, Eqs. (25) and (29b) become identical at $t=0$. Therefore, the condition $\ddot{a}_1(0)=0$ resulting from the condition of initial sphericity in bubble shape must be added to the numerical procedure.

The physical situation under consideration corresponds to a system temperature = 77°F, water density = 0.997 g/cm^3, surface tension for water-air system = 71.97 dyn/cm, $R(0)=1$ and $\dot{R}(0)=0$. The bubble is initially spherical. The dynamics of its growth or collapse while the bubble moves in three different flows is studied: a sink flow, a source flow, and a "sink-and-source" flow. The results are presented in Figs. 3–10.

Flow through a nozzle may approximately correspond to the physical situation of a sink flow if the bubble size is small in comparison with the cross sectional area of the nozzle. Figures 3 and 4 show the dynamic characteristics of a bubble moving in a sink flow for the initial conditions of $r_1(0)=105$, $R(0)=1.0$, $V_1(0)=200$, $\mu=2.2\times10^6$, and $p_{in}(0)=4395$. Under the specified conditions, the liquid and bubble velocities are assumed the same at the initial position of the bubble, $r_1(0)=105$. Numerical calculation was performed from $r_1(0)=105$ to $r_1(t)=100$, where the liquid is at saturation pressure. It is disclosed from Fig. 3 that both the velocity V_1 and the radius R increase monotonically with the bubble's position. The bubble's translatory velocity exceeds that of the liquid. Figure 4 shows the time history of the bubble shape. The bubble retains

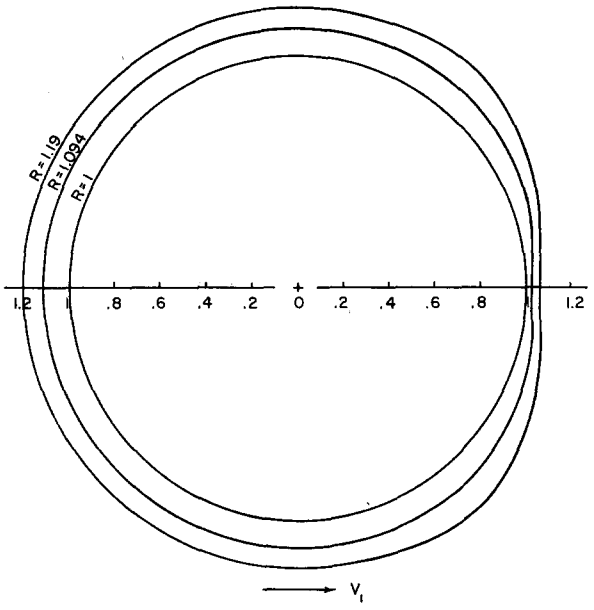

FIG. 4. The transient shape of an initially spherical bubble moving in a sink flow with the initial conditions $r_0=105$, $R(0)=1$, $V_0=200$, and $p_{in}(0)=4395$.

a spherical shape for a distance and then starts to flatten out at the downstream side.

In practice, flow through a diffuser may be approximated by a source flow. Figures 5–10 illustrate the dynamic characteristics of a bubble moving in a source flow with the initial conditions of $r_1(0)=100$, $R(0)=1.0$, $p_{in}(0)=195$, and $\mu=2.2\times10^6$. Some representative initial velocities between 240 and 260 were considered, although more cases corresponding to different initial velocities were studied in Ref. 8.

It was revealed from the study that the bubble's translating velocity and size may vary in two distinct manners depending upon the magnitude of the initial velocity $V_1(0)$. In other words, there exists a critical value for the initial velocity beyond which the bubble velocity and size may follow a different pattern. For

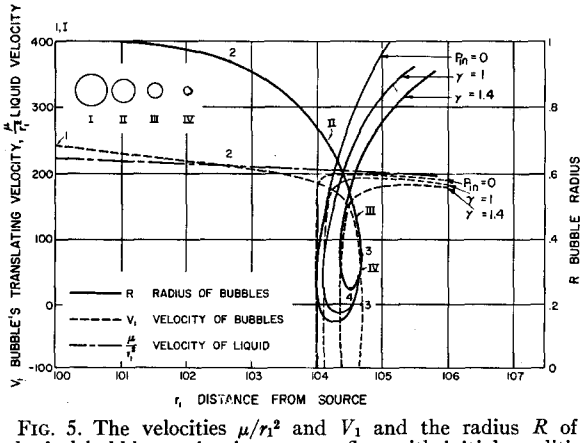

FIG. 5. The velocities μ/r_1^2 and V_1 and the radius R of a spherical bubble moving in a source flow with initial conditions $r_0=100$, $R(0)=1$, $V_0=240$ for three cases: (i) $p_{in}(0)=195$, $\gamma=1.4$, (ii) $p_{in}(0)=195$, $\gamma=1.0$, and (iii) $p_{in}(t)=0$. [The bubble shape is predicted by Eqs. (25) and (29).]

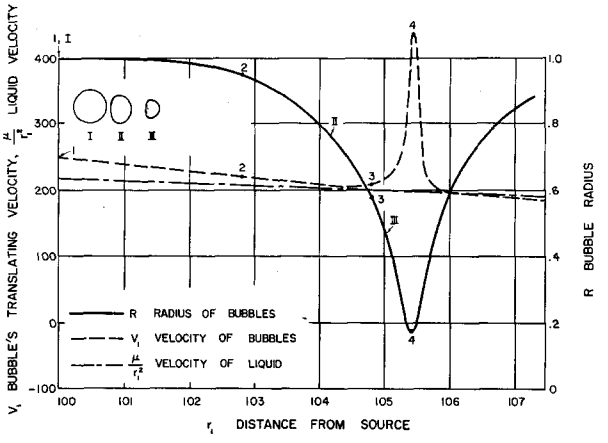

FIG. 6. The velocities μ/r_1^2 and V_1 and the radius R of a spherical bubble moving in a source flow with the initial conditions $r_0=100$, $R(0)=1$, $V_0=250$, and $p_{in}(0)=195$. [The bubble shape is predicted by Eqs. (25) and (29).] The value of γ is 1.4.

the parameters specified in the present study, the critical initial velocity is 249. When $V_1(0)$ is lower than 249, the bubble velocity and size vary following the pattern shown in Fig. 5, which is characterized by a "loop." Whereas, when $V_1(0)$ exceeds 249, these variations follow the other pattern as shown in Figs. 6 and 7, which is characterized by a "peak" or a "valley."

The variety of changes in the bubble shape in a source flow is due to the initial velocity $V_1(0)$. For small values of $V_1(0)$, the bubble first changes its shape from a sphere to an "ellipsoid," then indents on the downstream side and eventually forms a crater as shown in Fig. 8.

As the initial velocity increases the indentation shifts upstream along the bubble surface as shown in Fig. 9. When the initial velocity is further increased, the indentation occurs at the upstream side of the bubble surface as illustrated in Fig. 10.

Figure 11 shows the calculated time history of the velocity and radius of a spherical bubble traveling

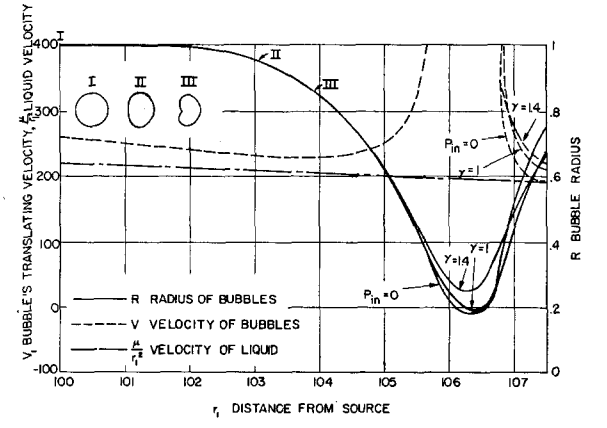

FIG. 7. The velocities μ/r_1^2 and V_1 and the radius R of a spherical bubble moving in a source flow with the initial conditions $r_0=100$, $R(0)=1$, $V_0=260$ for three cases: (i) $p_{in}(0)=195$, $\gamma=1.4$, (ii) $p_{in}(0)=195$, $\gamma=1.0$, and (iii) $p_{in}(t)=0$. [The bubble shape is predicted by Eqs. (25) and (29).]

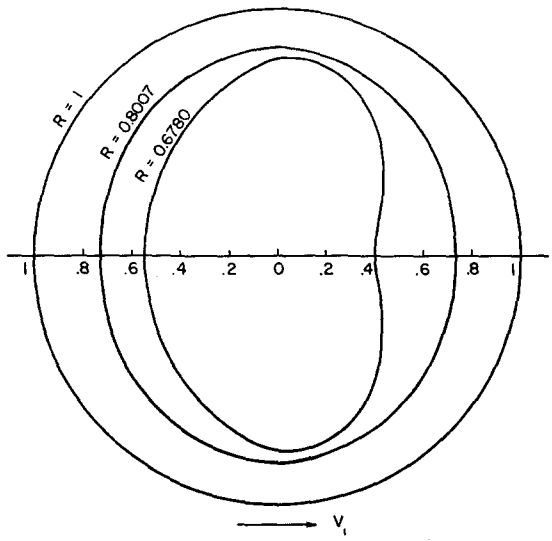

FIG. 8. The transient shape of an initially spherical bubble moving in a source flow with the initial conditions $r_0=100$, $R(0)=1$, $V_0=220$ for three cases: (i) $p_{in}(0)=195$, $\gamma=1.4$, (ii) $p_{in}(0)=195$, $\gamma=1.0$, and (iii) $p_{in}(t)=0$.

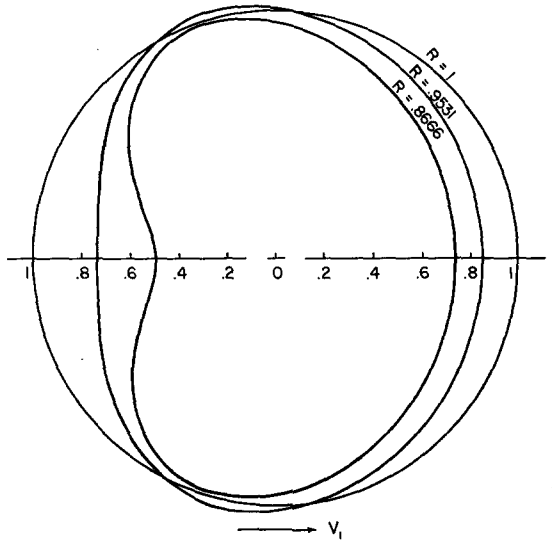

FIG. 10. The transient shape of an initially spherical bubble moving in a source flow with the initial conditions $r_0=100$, $R(0)=1$, $V_0=260$ for three cases: (i) $p_{in}(0)=195$, $\gamma=1.4$, (ii) $p_{in}(0)=195$, $\gamma=1.0$, and (iii) $p_{in}(t)=0$.

through a venturi tube. The liquid flow through the venturi tube may be approximated by the combination of a sink flow and a source flow of equal strength. The same initial conditions used for the sink flow case were also employed in this numerical solution. Also illustrated in Fig. 11 is the axial liquid-velocity distribution in the tube. $r_1=100$ corresponds to the location of the venturi throat. It is observed in the figure that the bubble grows quite rapidly after it passes the throat. It then starts to collapse. Figure 11 also indicates that the bubble may rebound at $r_1=107$ from the source. The process of rebounding followed by collapse repeats as the bubble moves downstream. The deceleration and acceleration of the bubble's translational motion also repeats. In practice, however, the bubble cannot remain spherical after it collapses to a certain size.

Mechanism: It was mentioned earlier that when a bubble travels in a source flow, its velocity and size vary with bubble position following two distinct patterns as shown in Figs. 5 and 6. The mechanism leading to these phenomena is discussed below. For convenience in discussion, the terms involving a_n in Eqs. (25) and (29a) are neglected since they do not contribute appreciably to the overall result. Then the equations can be rewritten as

$$d^2r_1/dt^2=-6\mu^2/r_1^5-3(\dot{R}/R)(V_1-\mu/r_1^2)-6(\mu/r_1^2)^2(R/r_1)^3R, \quad (30)$$

and

$$d^2R/dt^2=(1/2R)[(\mu/r_1^2)^2-(\mu/r_0^2)^2]+(1/4R)(V_1-\mu/r_1^2)^2-\tfrac{3}{2}\dot{R}^2/R+(p_{in}-p_0)/R-2/R^2+(5/3)(\mu/r_1^2)^2(R/r_1)^2, \quad (31)$$

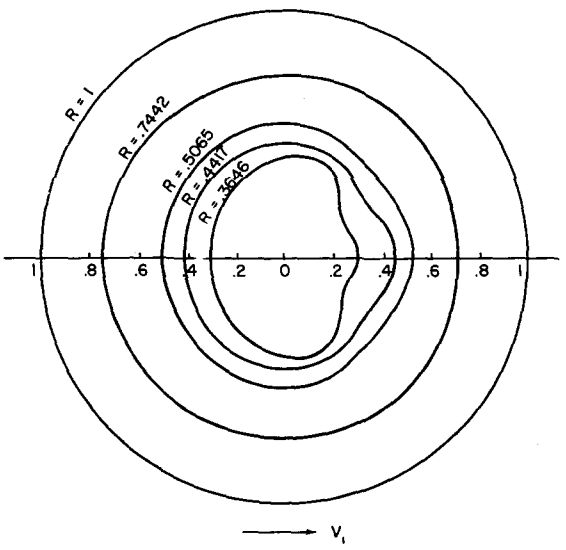

FIG. 9. The transient shape of an initially spherical bubble moving in a source flow with the initial conditions $r_0=100$, $R(0)=1$, $V_0=238$ for three cases: (i) $p_{in}(0)=195$, $\gamma=1.4$, (ii) $p_{in}(0)=195$, $\gamma=1.0$, and (iii) $p_{in}(t)=0$.

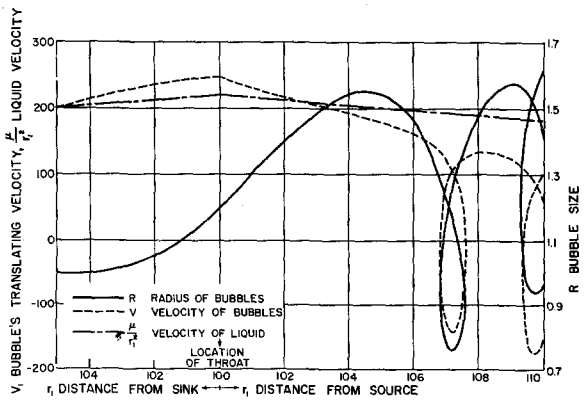

FIG. 11. The velocities μ/r_1^2 and V_1 and the radius R of a spherical bubble moving in a sink flow and then in a source flow with the initial conditions $r_0=105$, $R(0)=1$, $V_0=200$, and $p_{in}(0)=4395$. The value of γ is 1.4.

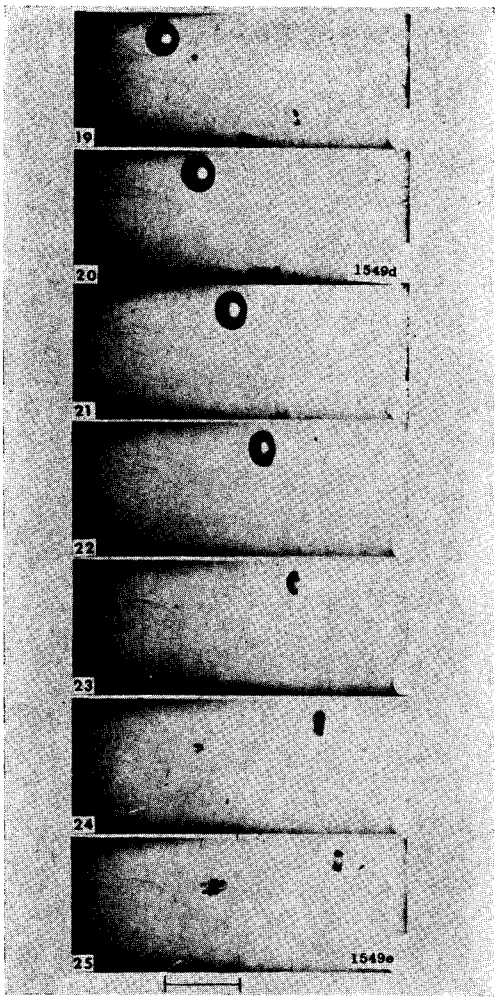

FIG. 12. High-speed photographs, $\frac{1}{4}$ in. venturi throat velocity 74.6 ft/sec, air content 2.35 vol%, 132 μsec/frame, scale length 0.25 in. [courtesy of ASME (Ref. 5)].

respectively. Equation (30) shows that the acceleration or deceleration of the bubble's translational motion consists of the components induced by μ^2/r_1^5 the liquid acceleration, by $(\dot{R}/R)(V_1-\mu/r_1^2)$, the interaction between $\dot{R}$ the rate of bubble growth or collapse, and $(V_1-\mu/r_1^2)$, the relative velocity between the liquid and the bubble, and by μ/r_1^2, the liquid velocity. Since the last component is of the third power of R/r_1, its contribution to the bubble's acceleration is negligible. Equation (31) indicates that the acceleration in the bubble growth or collapse consists of the components induced by the change in the liquid pressure with bubble position, by the relative velocity between the liquid and bubble, by the rate of bubble growth or collapse, by the pressure difference between the gas inside the bubble and the liquid at the initial position of the bubble, by the surface tension, and by the liquid velocity. The contribution of the last component is considered small, since it involves the second power of R/r_1.

Consider first the case where the initial velocity is smaller than the critical value. During the initial stage of the transient corresponding to the interval between points 1 and 2 in Fig. 5, the translational motion of the bubble is governed by the force induced by the deceleration of the liquid, while its collapse is controlled by the force induced by the change in the liquid pressure. However, as the bubble reaches point 2, the relative velocity between the bubble and the liquid changes its sign. As a result, the force induced by the interaction between the bubble's collapse rate and the relative velocity, the $-3(\dot{R}/R)(V_1-\mu/r_1^2)$ term in Eq. (30), becomes negative, which causes the bubble to further decelerate. As the bubble travels further downstream, the collapse rate continues to increase, thus causing an increase in the magnitude of the $-\frac{3}{2}\dot{R}^2/R$ term in Eq. (31). Therefore, the increases in the collapse rate and relative velocity interact to cause the bubble to further decelerate. This is indicated by a very rapid increase in the $-3(\dot{R}/R)(V_1-\mu/r_1^2)$ term in Eq. (30). The bubble velocity eventually becomes negative and the bubble starts to travel upstream when it reaches point 3 in Fig. 5. Meanwhile, the $(1/R)(V_1-\mu/r_1^2)^2$ term in Eq. (31) increases as the relative velocity increases. Since this term is always positive, it exerts a force to retard the collapse rate and eventually causes the bubble to stop collapsing when it reaches point 4 in Fig. 5. The bubble then starts to grow and travels upstream. This phenomenon may be called "rebound" or "regrowth" which was observed in various experiments.[5] At the moment of "rebound", the sign of $\dot{R}$ changes and the $-3(\dot{R}/R)(V_1-\mu/r_1^2)$ term in Eq. (30) becomes positive. This causes the bubble to accelerate so rapidly that the bubble velocity V_1 soon becomes positive and moves downstream again. However, as V_1 increases both the $V_1-\mu/r_1^2$ and $-3(\dot{R}/R)(V_1-\mu/r_1^2)$ terms tend to decrease. The latter term may eventually be exceeded by the decel-

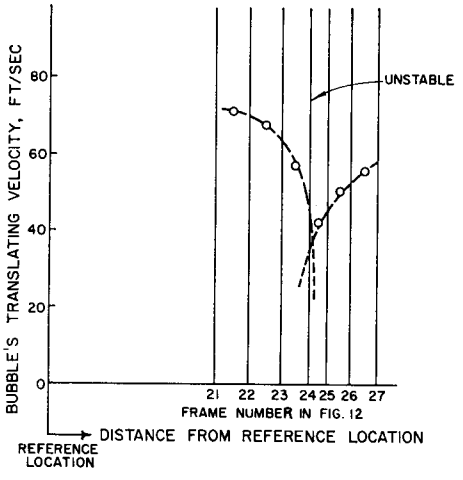

FIG. 13. Bubble traveling velocity vs its position in $\frac{1}{4}$ in. venturi throat (Fig. 12).

erating terms in Eq. (30). This is the reason why the bubble velocity is lower than the liquid velocity in the accelerating stage.

When the initial bubble velocity is greater than the critical value, the time history of the bubble velocity and size follows the second pattern as shown in Figs. 6 and 7. During the initial stage of the transient, corresponding to the interval between points 1 and 2, the bubble motion is governed by the deceleration of the liquid, while its collapse is controlled by the change in the liquid pressure. As the bubble travels downstream the collapse rate increases and the $-3(\dot{R}/R)(V_1-\mu/r_1^2)$ term in Eq. (30) becomes important. Since this term is positive, it tends to reduce the deceleration of the bubble motion. Before the bubble velocity is reduced to the magnitude of the liquid velocity, the magnitude of this term may become comparable to that of the $-6\mu^2/r_1^2$ term in Eq. (30) and eventually the bubble accelerates. This occurs at point 3 in Fig. 6. Meanwhile, the $-\frac{3}{2}\dot{R}^2/R$ term in Eq. (31) governs the bubble collapse like the first pattern. As the bubble is accelerated the relative velocity increases, as does the term $(1/4R)(V_1-\mu/r_1^2)^2$ in Eq. (31). As a result the bubble's collapse rate decreases. At point 4 in Fig. 6 the bubble stops collapsing and starts to grow; but due to the sign change in the $-3(\dot{R}/R)(V_1-\mu/r_1^2)$ term, the bubble velocity is decreased.

It is disclosed from the numerical raduction that in the vicinity of point 3 where both $V_1-\mu/r_1^2$ and $\dot{R}$ are large, a_n increase very rapidly and soon become too large to be applicable to the perturbation method. Physically, this moment corresponds to the threshold of instability where the bubble becomes highly irregular shape.

The gas pressure inside the bubble plays a relatively important role only when the bubble size is small. Although the presence of gas may somewhat contribute to the cause of "rebound", it is the $(1/4R)(V_1-\mu/r_1^2)^2$ term in Eq. (31) which plays more important role on the "rebound" phenomenon.

In order to examine the influence of the presence of a gas inside the bubble and its thermodynamic behavior on the dynamic behavior of the moving bubble, three representative cases were compared in Figs. 5, 7–9, and 10. These three cases are (i) $p_{in}(0)=195$, $\gamma=1.4$ which corresponds to an adiabatic process, (ii) $p_{in}(0)=195$, $\gamma=1.0$ which is an isothermal process and (ii) $p_{in}(t)=0$ which corresponds to the absence of a gas within the bubble. It is seen from these figures that during the course of bubble collapse, from its inception to the threshold of instability, the presence of the gas and its thermodynamic behavior do not affect the translating velocity, unperturbed radius and instantaneous shape of the bubble. It is most important to note that the "rebound" phenomenon occurs even in the absence of a gas within the bubble as shown in Figs. 5 and 7.

A photographic study for the dynamics of a cavitation bubble traveling through a $\frac{1}{4}$ inch venturi throat was performed in Ref. 5. One representative result was reproduced here in Fig. 12. The bubble velocity vs its position shown in Fig. 12 is plotted in Fig. 13. It must be denoted that since the venturi is rectangular in cross section, the flow may be approximated as a two-dimensional source flow (from a line source). However, Fig. 12 indicates that the instability in bubble shape begins at the moment when the rate change in the translating velocity is maximum. The mechanism is in agreement with the present analysis for the point-source flow.

CONCLUSION

The following conclusions are made from the present study:

(1) When a gas bubble is in translatory motion, the bubble may be accelerated or decelerated as the result of the relative velocity between the bubble and the liquid and the rate of bubble collapse or growth. In addition, the relative velocity between the bubble and the liquid may accelerate the rate of growth.

(2) The time history of the bubble's translating velocity in a sink flow monotonically increases, while in a source flow it varies following two typical patterns depending on the initial velocity. When the initial velocity is smaller than a critical value, the translating motion of the bubble is decreased as it collapses. After the bubble comes to a complete stop, it travels upstream for a short distance, then moves downstream, growing again. When the initial velocity is greater than the critical value, the bubble's translating motion is first decreased as it collapses. The velocity is then increased over a short distance followed by a deceleration and a regrowth of the bubble.

In a sink flow, an initially spherical bubble can maintain a nearly spherical shape over a rather long distance as it grows. In a source flow, the bubble shape varies with time in various ways depending upon the initial velocity. When the initial translating velocity is low, the initially spherical bubble becomes oblate in shape. It then flattens on the downstream side. As the initial velocity increases, the indentation shifts upstream along the bubble surface. When the initial velocity is further increased, the indentation occurs on the upstream side. During the collapse the bubble shape may become unstable when the rate change in the translatory velocity is large.

(3) The characteristic features in the dynamic behavior of a translating gas bubble as described in the previous sections were previously disclosed in the photographic study of a cavitation bubble in a rectangular venturi tube.[5]

The first author is grateful to Professors J. A. Clark, F. G. Hammitt, and J. D. Murray for their encouragement and advice.